Computers and Concrete, *Vol. 26, No. 1* (*2020*) *11-20*
DOI: https://doi.org/10.12989/cac.2020.26.1.011

Research on damage of 3D random aggregate concrete model under ultrasonic dynamic loading

Lixiao Wang[1,2], Qidong Chen[1], Xin Liu*[1], Bin Zhang[1] and Yichen Shen[2]

[1]*School of Mechanical Engineering, Changshu Institution of Technology, Changshu, 215500, China*
[2]*School of Mechanics, Soochow University, Suzhou, 215000, China*

(*Received November 26, 2019, Revised April 30, 2020, Accepted May 18, 2020*)

Abstract. Concrete are the most widely used manmade materials for infrastructure construction across the world. These constructions gradually aged and damaged due to long-term use. However, there does not exist an efficient concrete recycling method with low energy consumption. In this study, concrete was regarded as a heterogeneous material composed of coarse aggregate and cement mortar. And the failure mode of concrete under ultrasonic dynamic loading was investigated by finite element (FE) analysis. Simultaneously, a 3D random aggregate concrete model was programmed by APDL and imported into ABAQUS software, and the damage plastic constitutive model was applied to each phase to study the damage law of concrete under dynamic loading. Meanwhile, the dynamic damage process of concrete was numerically simulated, which observed ultrasonic propagating and the concrete crushing behavior. Finally, the FE simulation considering the influence of different aggregate volume and aggregate size was carried out to illustrate the damage level of concrete.

Keywords: concrete; ultrasonic; random aggregate model; damage plastic; numerical simulation

1. Introduction

As the most commonly used engineering composite material, concrete is widely used in urban roads and infrastructure constructions due to its versatility in shape and form, relatively low price, structural properties and abundance. Concrete structures may be subjected to different dynamic or static loading, which causes inevitable damage in its long-term operation. Eventually the abandoned concrete structures destroy the surrounding ecological environment and even threaten social security. Therefore, the recycle of waste concrete is very important for environmental protection (Kaliyavaradhan *et al*. 2017), so it is necessary to study the mechanical properties of concrete materials under various loading.

With regard to the demolition of abandoned concrete structures, the former researchers have done many important works. Jin (2019) discussed the legislation and practice of concrete recycling in the United States and other countries in terms of case analysis, which provided a theoretical and practical basis for concrete recycling. Salesa (2017) proved the feasibility of recycled self-compacting concrete from precast concrete waste products by using the rheological and the slump-flow test. It was indicated that the excellent physical and mechanical properties of recycled concrete were friendly to environment. Kalinowska (2020) used thermal and mechanical treatment to disintegrate the mortar. The optimal processing parameters of concrete crushed stone was determined by separating the hardened cement mortar and coarse aggregate. Lotfi (2015) carried out multi-stage procedure of the concrete rubble. Advanced technology was utilized to produce cement and clean aggregates from construction waste, and highly purify coarse aggregates from the old mortar. However, in the previous studies, the efficiency was not taken into consideration. The process of waste concrete recycling and regeneration was too cumbersome and the desired results could not be achieved. So the ultrasonic concrete crushing technology proposed in this paper is expected to become a new research in future for concrete recycling due to its high efficiency and good directionality.

Recently, the studies on the damage mechanical properties of concrete have been conducted. Relevant studies have shown that ultrasonic spreads in concrete generally propagate in the form of stress waves (Nakahata *et al*. 2015). In the experiment, it is difficult to observe the microcosmic failure process, while the numerical simulation can be presented visually and provide numerical guidance for the test. Wittmann (1988) first proposed the numerical simulation method to analyze the damage mechanical properties of concrete at the microscopic level. Bazant (1990), on this basis, created a random particle model to study concrete damage and microscopic crack growth process. Therefore, more and more researchers began to study the dynamic mechanical properties of concrete. Zhou (2016) established a two-dimensional concrete FE model to simulate its dynamic tensile behavior. The proposed model was validated by comparison between the experimental and numerical data. Kwak (2015) and Kim (2019) simulated the concrete failure process under the condition of high strain rate. The structural behavior was investigated through the failure modes and cracking patterns. The results showed damage resistance

*Corresponding author, Ph.D.
E-mail: liuxin2174897@163.com

http://www.techno-press.org/?journal=cac&subpage=8
ISSN: 1598-8198 (Print), 1598-818X (Online)

enhancement with the increase of concrete strength. As mentioned above, the dynamic constitutive model is the basis for the research of concrete dynamic mechanisms, and it also plays an important role in the analysis and mechanical behavior of concrete. However, these studies did not consider the integral mechanical properties of concrete, and only discussed its tensile and compressive damage properties in two dimensions. In addition, little research has considered the mechanical properties of concrete in three dimensions. Zhang *et al.* (2016) presented study aims at developing a versatile constitutive framework for concrete, which could be used in various stress states. Then a 3D elastoplastic damage model was developed based on the construction of plastic damage function. The asphalt concrete was regarded as an inhomogeneous material with fine aggregate matrix, Chen (2017, 2018) proposed a random algorithm to establish a three-dimensional FE model of asphalt concrete. The FE method was used to predict the dynamic modulus of models with different structures, and the results verified its effectiveness. Tehrani (2013) used maxwell model to describe the matrix's viscoelastic behavior. A three-dimensional digital model was established and the complex modulus of asphalt concrete was predicted considering granular aggregates. However, the influence of aggregate shape was not investigated. Meanwhile, the aggregate shape was regarded to be circular without considering the real aggregate shape in previous researches.

Previous research on the dynamic characteristics of concrete was mainly divided into single impact (Xiang *et al.* 2017, Yu *et al.* 2014, Saleem *et al.* 2016), low frequency vibration (Zhang *et al.* 2018, Cao *et al.* 2018) and blasting (Nam *et al.* 2009, Li *et al.* 2018). However, in some recent studies, drop hammer and Hopkinson pressure bar (SHPB) tests are the most popular techniques for dynamic characterization of concrete strain rate (Gultop *et al.* 2015, Gholipour *et al.* 2019, Heravi *et al.* 2020). Al-Salloum *et al.* (2015) tested the dynamic behavior of concrete experimentally using annular and solid concrete specimens by split Hopkinson pressure bar (SHPB). Results show that failure modes of concrete is typical high strain rate ductile failure and low strain rate brittle failure. Wu (2017) studied the dynamic damage mechanical properties of concrete subjected to spiral impact. Aoude (2015) and Yu (2014) used ultra-high performance fiber reinforced concrete to study its performance under explosive impact loading. Anil (2016) conducted experimental and numerical investigations on different types of reinforced concrete beams under impact loading. It was found that the material type has an effect on the width of the crack. Comparatively, there are few researches on the damage of three-dimensional concrete model with random aggregate under ultrasonic dynamic loading.

In this paper, concrete was regarded as a heterogeneous composite material composed of cement mortar and coarse aggregate (Nakahata *et al.* 2015, Wittmann 1988, Wang *et al.* 2015). Considering aggregate shapes, aggregate was set as random polygon to avoid excessive time consumption. The three-dimensional random aggregate model of concrete was programmed by APDL, and then, the model was imported into ABAQUS software. According to the excellent nonlinear simulation ability of the Explicit/Dynamic module in ABAQUS, the effects of ultrasonic amplitude, coarse aggregate volume fraction and particle size on concrete's mechanical properties under dynamic ultrasonic loading were studied.

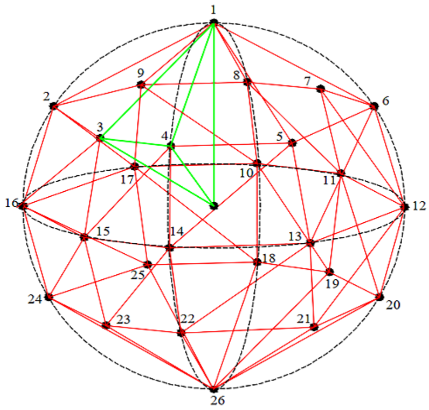

Fig. 1 Three-dimensional spherical aggregates

2. Random aggregate generation and release program

2.1 The generation method of random aggregate numerical simulation procedure

Any point P in three-dimensional polar coordinate, can be determined by r, θ, φ three parameters (Wang *et al.* 2015) (where r is the radius of point P, θ is the angle between point P and the positive Z-axis, φ is the angle between the line from the origin to point P in the XY-plane and the positive X-axis). The generation method is as follows: (1) Generate spherical aggregate frame, on this basis, its central coordinates (x, y, z) and radius D are taken as the control parameters of the location and size of random aggregate (Skarzynski *et al.* 2015). (2) 26 points are set in every 45° intervals of θ or φ directions on the sphere and mark the number. By connecting these points, their surfaces can be approximately combined into a spherical area, as shown in Fig. 1. (3) The 26 points on the spherical aggregate frame are nodes which can fluctuate randomly with respect to the initial position, so the generation of random aggregates can be realized. (4) Assume that one point in the node is k, and the initial parameter of the point is r_{ki}, θ_{ki}, φ_{ki}. In order to avoid the formation of excessively deformed aggregate, the fluctuation of aggregate particle size r is set in the range (0, D/2), and θ, φ are set in the range (0°, 22.5°), so the aggregate vertex function can be expressed as:

$$\begin{cases} r_k = r_{ki} + f_r \cdot \mathrm{random}(-1,1),\ f_r \in (0, D/2) \\ \theta_k = \theta_{ki} + f_\theta \cdot \mathrm{random}(-1,1),\ f_\theta \in (0^\circ, 22.5^\circ) \\ \varphi_k = \varphi_{ki} + f_\varphi \cdot \mathrm{random}(-1,1),\ f_\varphi \in (0^\circ, 22.5^\circ) \end{cases} \quad (1)$$

where random (-1, 1) is a random function, which means generating a random number between (-1, 1).

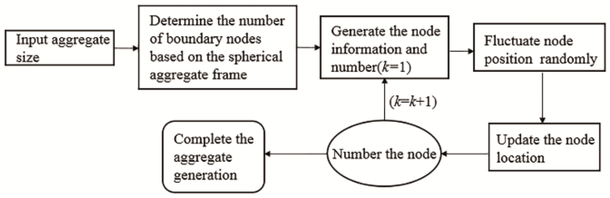

Fig. 2 Flow chart of random concrete aggregate

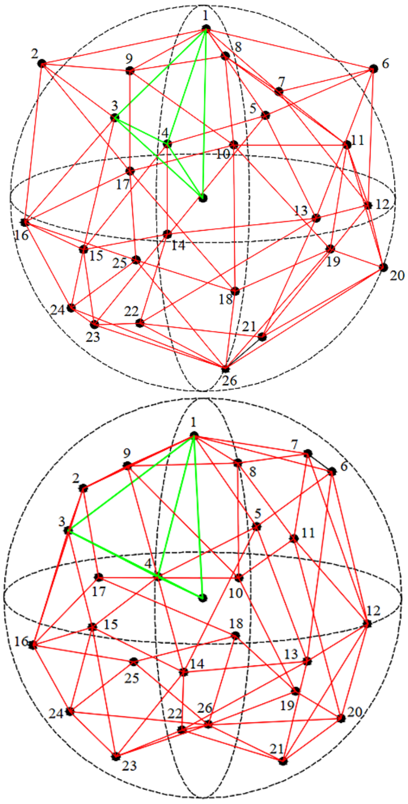

Fig. 3 Three-dimensional aggregates with arbitrary shapes

The aggregate generation process is shown in Fig. 2. When the aggregate node fluctuates in the direction of r, θ, φ according to Eq. (1), random aggregate can be obtained, as shown in Fig. 3.

2.2 Aggregate release and model generation

After the aggregates have been generated, database of aggregate was generated according to the gradation required by the project (Huang *et al*. 2015). In the actual production projects, aggregate is divided into continuous grade and single grain grade. Single grain grade is usually divided into four grades. In this article, aggregate was set as the one graded (The aggregate size of the one grade is 5-20 mm). The next step was to distribute the built aggregate model into the concrete frame (Abyaneh *et al*. 2013): (1) Create the geometric model in the APDL. (2) Put the generated aggregate into the geometric model and make the distance between two aggregates larger than the sum of the radius of them ($\sqrt{((x_1-x_2)^2+(y_1-y_2)^2+(z_1-z_2))^2} > \frac{3}{2}(\mathrm{D}_1+\mathrm{D}_2)$, x_1, y_1, z_1 is the central coordinate of aggregate 1; x_2, y_2, z_2 is the central coordinate of aggregate 2; D_1 is the radius of aggregate 1, D_2 is the radius of aggregate 2), so as to prevent the mutual invasion of aggregates and loss of the model accuracy. (3) Put aggregate according to the required volume fraction. Table 1 shows the statistical results of the release algorithm, and in this paper, the size of coarse aggregate was set as 5-20 mm. The final generated 3D aggregate model is shown in Fig. 4. (4) Import the generated concrete model into ABAQUS.

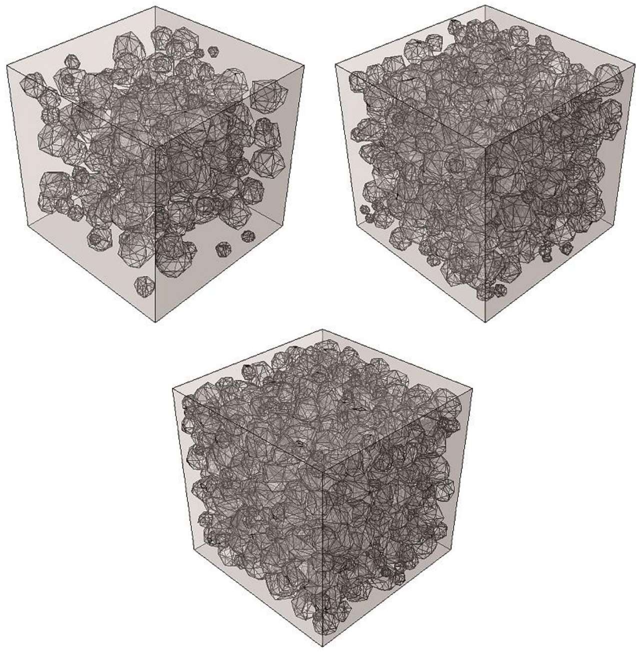

Fig. 4 Concrete models with different aggregate volumes

Table 1 Statistical results (one graded)

Aggregate size (mm)	Objective volume 20%		Objective volume 40%		Objective volume 60%	
	Actual number	Placed volume ratio	Actual number	Placed volume ratio	Actual number	Placed volume ratio
5~20	190	20%	436	40%	595	60%

3. Finite element analysis

3.1 The simulation model

The damage analysis of concrete under ultrasonic is a typical nonlinear process, usually accompanied by obvious softening stage (Tahmouresi *et al*. 2019, Liu 2009). However, the conventional implicit analysis method is difficult to effectively solve these problems, so the damage process of concrete under ultrasonic is solved by the explicit dynamics calculation (Zhou *et al*. 2016, Kwak 2015, Kim *et al*. 2019, Liu 2009, Smith *et al*. 2014). In this paper, the damage plastic effect of 3D random aggregate concrete under ultrasonic dynamic loading was simulated under the Dynamic/Explicit module of ABAQUS. Three FE models of different sizes were adopted, which were cubes with side of 75 mm, 100 mm and 150 mm respectively. The

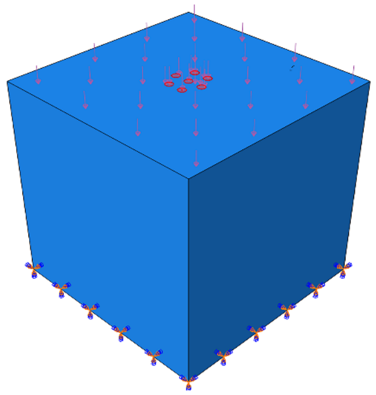

Fig. 5 Three-dimensional FE model of concrete

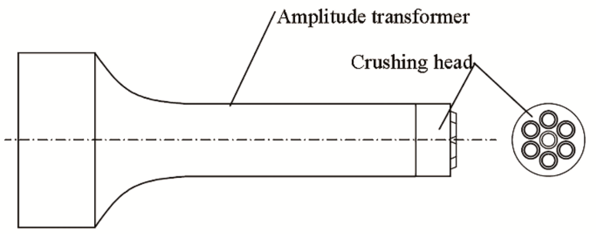

Fig. 6 Broken tool structure

FE model in Fig. 5 shows a model with side of 100 mm where the volume fraction of coarse aggregate is 40%, and the particle size is 5-20 mm. In order to save calculation time and retain calculation accuracy, the mesh size of coarse aggregate and cement mortar was set as 2 mm (Alexandre 2013, Du *et al*. 2014).

The setting of the boundary conditions is shown in Fig. 5. Fixed constraints were applied at the bottom of the 3D concrete model and a static load was applied on the top surface of the concrete model. By applying the stress wave of ultrasonic on the red circular lattice area which use the broken tool as shown in Fig. 6, the simulation of the ultrasonic dynamic loading was carried out. Each phase adopted binding constraint to ensure the force transfer of each phase after the failure of the element. Ultrasonic loading of crushed concrete is a complex non-linear process. In order to better simulate this process, two steps were established under the Dynamic/Explicit module. The first static load was set as 5 MPa at the first step to complete pretension. The second step was loaded with ultrasonic dynamic loading, and the amplitude ranges from 0 to 25 MPa. In the numerical simulation process, the amplitude curve of ultrasonic dynamic loading was defined as ultrasonic signal with a frequency of 20 kHz.

3.2 Material model

3.2.1 Concrete damage plastic constitutive model

The concrete damage plastic model of ABAQUS proposed by Matzenmiller *et al*. (1995) was applied in this study, which is convenient for the damage study of concrete structures (Abdollahzadeh *et al*. 2016).

The effective stress of damage is

$$\bar{\sigma} = (1-d)\sigma \tag{2}$$

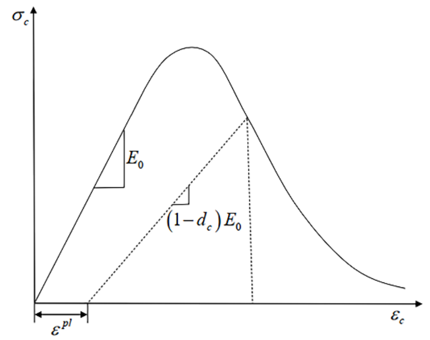

Fig. 7 Curves of compressive stress and strain of concrete

where $\bar{\sigma}$ is the effective stress, d is the damage factor, its value varies from 0 to 1, which represents the change from undamaged to failure.

The relation between effective stress and elastic stress is as follows

$$\sigma = D_0^{el}\left(\varepsilon - \varepsilon^{pl}\right) \tag{3}$$

where D_0^{el} is the undamaged initial stiffness of the material, ε^{pl} is the plastic strain. Scalar expression of stress-strain relation

$$\bar{\sigma} = (1-d)D_0^{el}\left(\varepsilon - \varepsilon^{pl}\right) \tag{4}$$

d_c represents the stiffness degradation ratio of concrete under compression (Ganesan *et al*. 2013, Liu *et al*. 2019), and the uniaxial stress can be expressed as

$$D_c = (1-d_c)D_0^{el} \tag{5}$$

According to Eq. (5) as well as Fig. 7, after the concrete is damaged, the initial unloading stiffness E_0 is degraded into $(1-d_c)E_0$.

3.2.2 The value of damage factor

In order to expound the relationship between internal damage and stress in concrete, the parameter of damage factor-inelastic strain curve should be provided (Du *et al*. 2014, Matzenmiller *et al*. 1995). The related parameters of damage factor can be calculated by energy equivalence principle. The elastic residual energy generated by stress on damaged materials and undamaged materials is in the same form, so the stress and the elastic modulus is changed to the equivalent stress and the equivalent elastic modulus respectively (Kim *et al*. 2013, Liang *et al*. 2017).

Undamaged elastic residual energy

$$W_{0^e} = \frac{\sigma^2}{2E_0} \tag{6}$$

Equivalent damage elastic residual energy

$$W_{d^e} = \frac{\bar{\sigma}^2}{2E_d} \tag{7}$$

And because

$$\bar{\sigma} = (1-d)\sigma \tag{8}$$

Table 2 Model parameters

Material	Modulus of elasticity (GPa)	Poisson's ratio	Bulk density (t/m^3)	Expansion Angle (ψ)	Flow potential offset (ε)	Constant tress ratio (K_c)	Ratio of double and uniaxial compressive strength (α_f)
aggregate	23	0.167	2.6				
mortar	10.66	0.2	2.1	35	0.1	0.667	1.16

(a) Concrete crushing experiment results (b) Concrete damage simulation

Fig. 9 The comparison of concrete crushing experiment and simulation

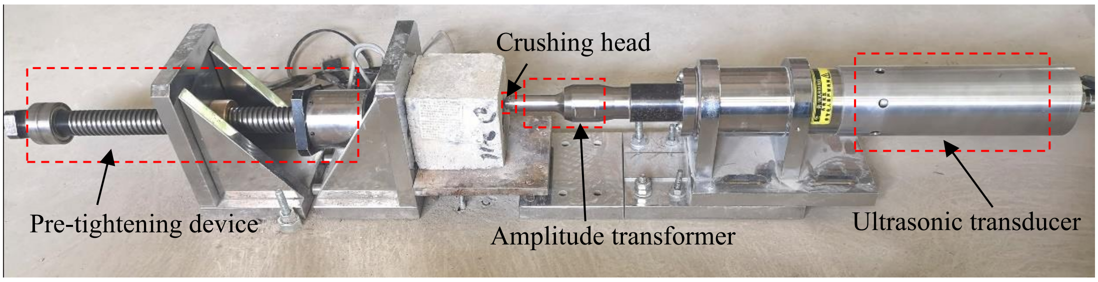

Fig. 8 Ultrasonic crushing unit

Then E_d=E_0(1−d)^2 can be obtained, which can be further concluded as follows

$$\sigma = E_0 \left(1-d\right)^2 \varepsilon \tag{9}$$

The calculation formula of uniaxial compression damage factor is as follows

$$d=\begin{cases} 1-\sqrt{k_c\left[\alpha_c+\left(3-2\alpha_a\right)x+\left(\alpha_c-2\right)x^2\right]} & x\le 1 \\ 1-\sqrt{k_c\Big/\left[\alpha_c\left(x-1\right)^2+x\right]} & x>1 \end{cases} \tag{10}$$

where $x=\varepsilon/\varepsilon_c$, $k_c = f_c^* / \left(\varepsilon_c E_0\right)$. α_a and α_d are calculated from the stress-strain curve of concrete under uniaxial compression. According to Eq. (10), the damage factor required by ABAQUS damage plastic model can be calculated.

3.2.3 Model parameters and test results

The basic parameters of the model for cement mortar and coarse aggregate suggested by Liu (2009, 2016) was adopted and modified in this paper which is shown in Table 2. The damage factor and parameters of concrete damage plastic model were calculated at the part 3.2.2. The linear elastic model was used to describe the stress-strain relationship because of the high strength and fracture energy of the aggregate and the concrete damage plastic model was used to describe the property of mortar due to its well non-linear characteristics (Asteris *et al*. 2019).

The comparison results of concrete damage and simulation under ultrasonic loading is shown in Fig. 9, and the ultrasonic crushing unit is shown in Fig. 8. In the simulation, the size of the specimen, the volume fraction of coarse aggregate and the particle size were consistent with the experiment. It can be seen that the macroscopic failure of the experiment present partial or complete failure at the top of model, and the simulation results show the similar results.

3.2.4 Validation of constitutive model

The experimental and numerical simulation of concrete peak stress comparison is shown in Fig. 10. Ensure that the aggregate volume fraction of each model was 40%, and the coarse aggregate particle size was 5-20 mm. Experiments and numerical simulations measured the relationship between the peak stress of concrete under the same size model respectively. When the amplitude of ultrasonic peak stress is 3 MPa, 5 MPa, 10 MPa, 15 MPa, 20 MPa, 30 MPa respectively, the error of numerical simulation and experiment results of the same model are shown in Table 3. It can be seen that due to the difference of actual size of concrete and numerical simulation, there are inevitable errors in size and aggregate volume fraction. Therefore, the relative errors are more obvious when the loading force is

Table 3 Data errors

Size of concrete (mm)	The error in numerical simulation and experiment results (%)					
	3 MPa	5 MPa	10 MPa	15 MPa	20 MPa	30 MPa
75×75×75	18.15	-18.66	-4. 56	5. 79	5.09	4.35
100×100×100	-14.39	-11.66	-16.66	-9.72	3.12	-0.44
150×150×150	-60.12	-43.22	-5.11	-0.08	-2.34	-5.36

not so large; however, when loading force increases, the concrete stress state stabilizes gradually, resulting in a reduction in errors. According to the above discussion, the numerical simulation is in good coordinate with the experimental results, so the FE model and the selected model parameters established in this study are reliable and can be further utilized.

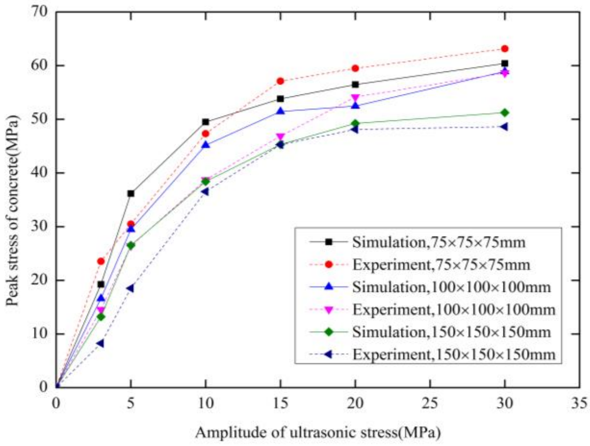

Fig. 10 Comparison of peak stress of concrete: experiment versus numerical simulation results

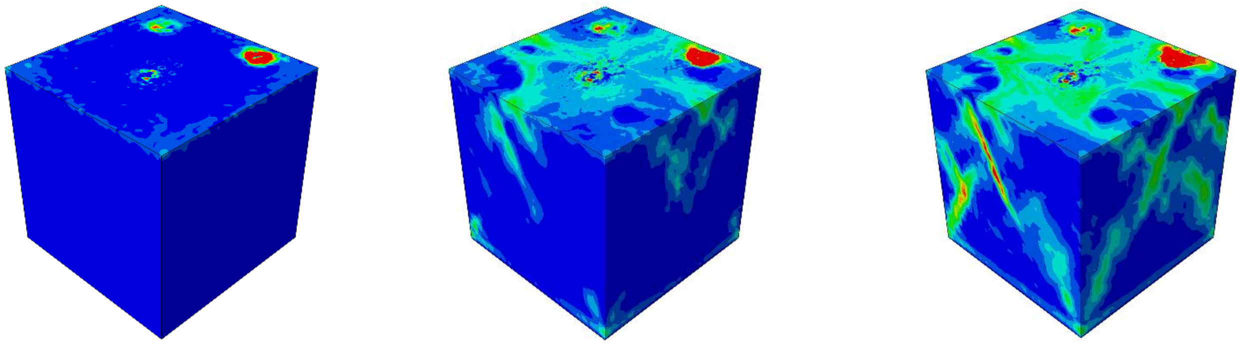

50μs 150μs 200μs

(a) 100 mm×100 mm×100 mm, 40%, 5-20 mm, P=5 MPa

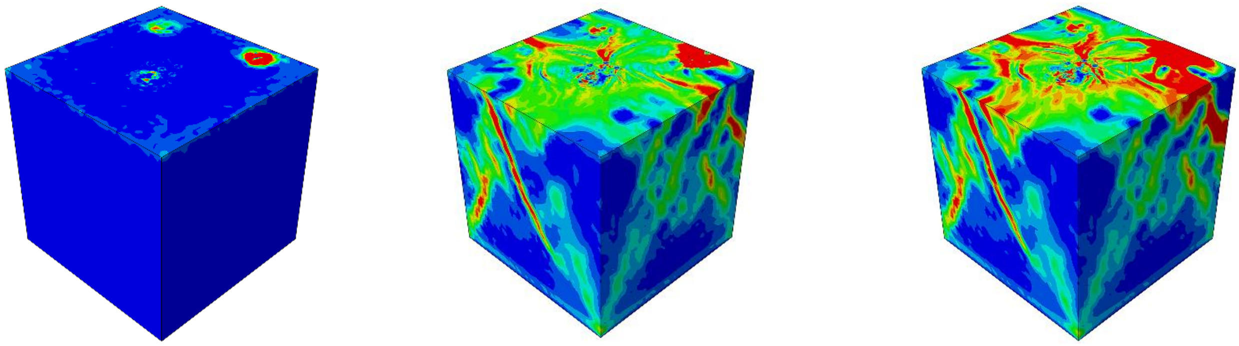

50μs 150μs 200μs

(b) 100 mm×100 mm×100 mm, 40%, 5-20 mm, P=15 MPa

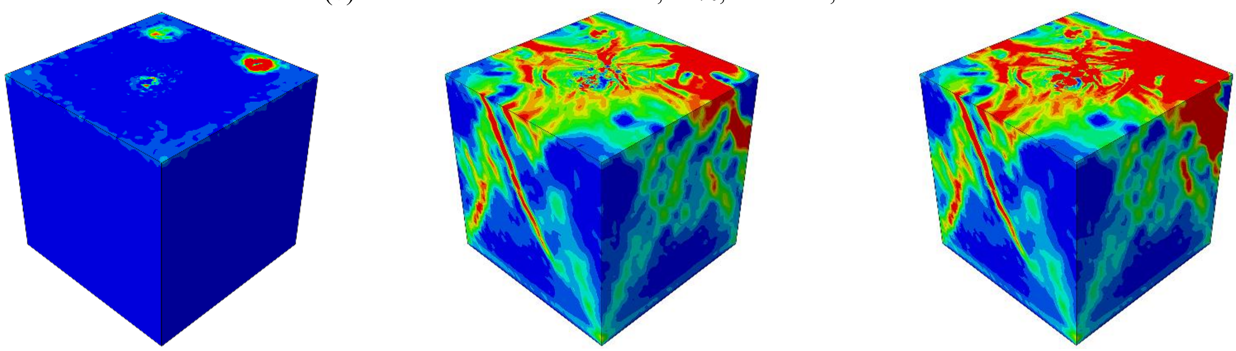

50μs 150μs 200μs

(c) 100 mm×100 mm×100 mm, 40%, 5-20 mm, P=30 MPa

Fig. 11 Concrete damage process

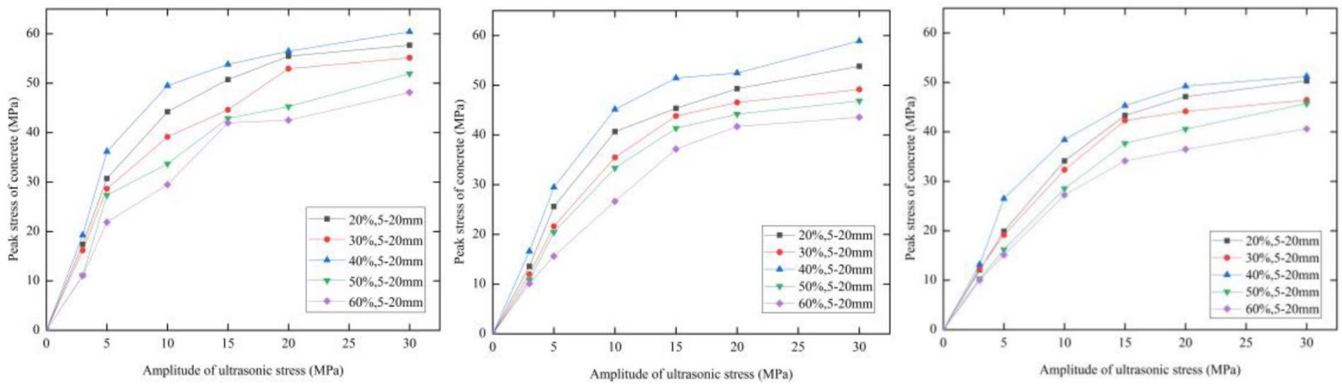

(a) Cube with side of 75 mm (b) Cube with side of 100 mm (c) Cube with side of 150 mm

Fig. 12 The relationship between peak stress of concrete and amplitude of ultrasonic stress

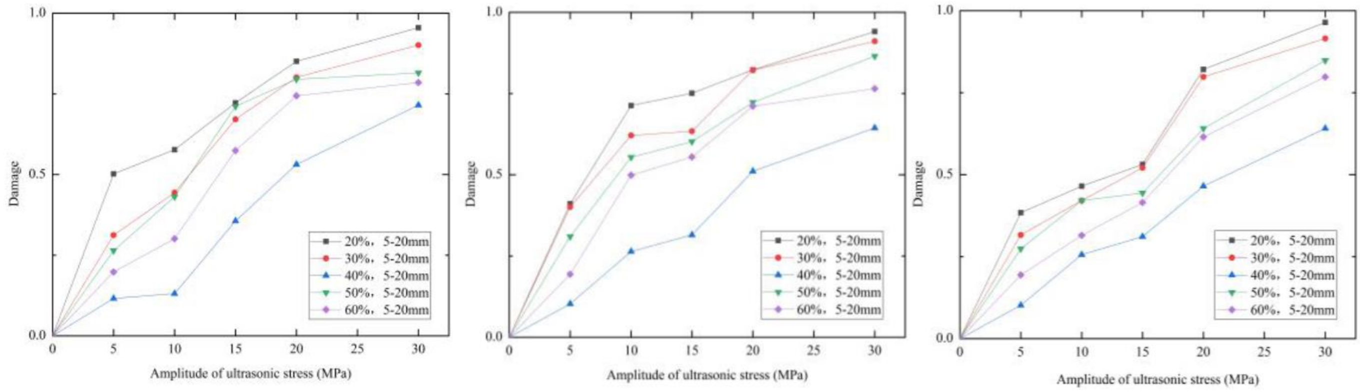

(a) Cube with side of 75 mm (b) Cube with side of 100 mm (c) Cube with side of 150 mm

Fig. 13 The relation between the volume fraction of coarse aggregate and concrete damage

4. Analysis of numerical simulation results

4.1 Damage failure mode of concrete

For ultrasonic concrete crushing specimens made of one graded aggregate, the relevant FE model was established. In the model, the size of concrete is a cube with side of 100 mm. Besides, the content of coarse aggregate in the established model is 40%, which is the same as the designed experimental specimen, and the particle size of coarse aggregate is 5-20 mm as shown in Fig. 11. When the amplitude of ultrasonic stress reaches 5 MPa, due to the pre-pressure, only partial damage generates on the concrete surface without obvious changes. As well as the amplitude of ultrasonic is 15 MPa, the concrete damages obviously, and the damage area forms into thin strips and pieces. Since that the damage energy generated by ultrasonic is not enough to cause the damage of concrete before reaching the bottom, and then, part of the damage energy reflects back to the top of the specimen, which strengthens the stress and strain field at the top and promotes the generation and expansion of new damage zone. While, the damage area has become a integrated area when the amplitude is loaded to 30 MPa. The damage starts from the incoming area of the ultrasonic superposition and spreads downward. It can be seen that under the same loading time, the larger the amplitude is, the more obvious the damage is.

4.2 Influence of amplitude of ultrasonic stress

The influence of ultrasonic stress with different specimens size is shown in Fig. 12, also the damage failure process of concrete with different aggregate volume and the influence of amplitude of ultrasonic on its peak stress are analyzed. It can be seen that, with the increase of the amplitude of ultrasonic stress, the peak stress of concrete increases gradually. While in the same model, the peak stress of the concrete model with 40% coarse aggregate volume fraction reaches the maximum value, and it is also applicable to different model size. Furthermore, it can be concluded that, with the increase of model size, the peak stress of concrete decreases, which has obvious size effect.

4.3 Influence of volume fraction of coarse aggregate on concrete damage

Considering the concrete specimens with different size as the simulation model, the effect of coarse aggregate volume fraction on concrete damage characteristics was analyzed under the terms of increasing amplitude. As shown in Fig. 13, the particle size of coarse aggregate is determined as 5-20 mm, and the volume fraction of coarse aggregate changes from 20% to 60%. With the increase of amplitude of ultrasonic stress, the damage value of concrete under dynamic loading gradually increases. As the volume

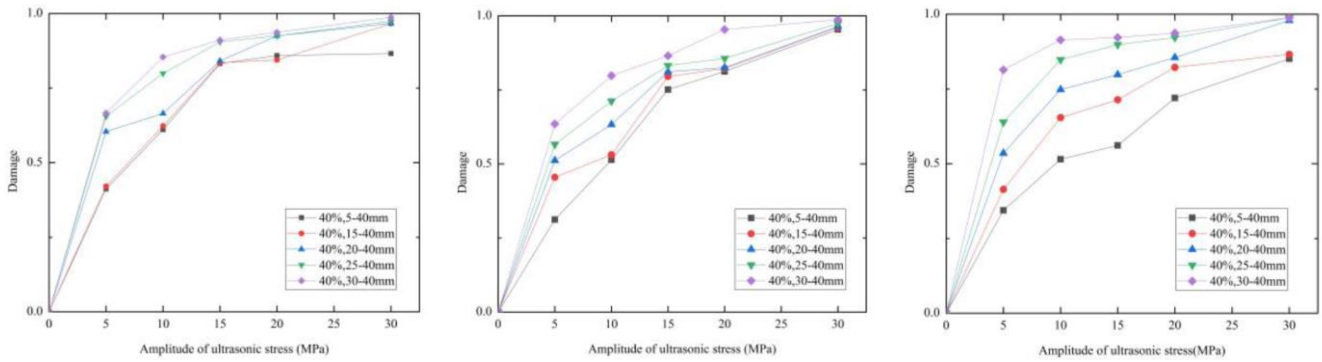

(a) Cube with side of 75 mm (b) Cube with side of 100 mm (c) Cube with side of 150 mm

Fig. 14 The relation between the minimum particle size of concrete coarse aggregate and concrete damage

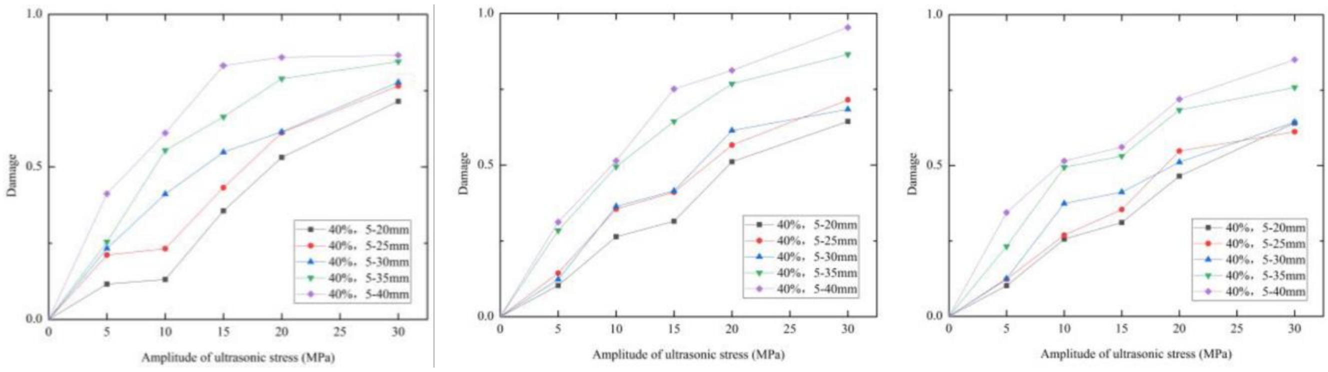

(a) Cube with side of 75 mm (b) Cube with side of 100 mm (c) Cube with side of 150 mm

Fig. 15 The relation between the maximum particle size of concrete coarse aggregate and concrete damage

fraction of coarse aggregate reaches 40%, the anti-damage ability is shown to be the best. Similarly, the horizontal comparison reveals that the damage value of concrete model decreases slowly with the increase of model size.

4.4 Influence of volume fraction of coarse aggregate on concrete damage

4.4.1 The minimum particle size of coarse aggregate

In order to study the effect of the minimum particle size of coarse aggregate on concrete damage, the dynamic damage simulation was carried out on concrete specimen under the premise of ensuring the maximum particle size of coarse aggregate 40 mm, where the minimum particle size of coarse aggregate distributed within the range of 5-30 mm. As is shown in Fig. 14, with the amplitude of ultrasonic stress increases, the damage value of concrete increases gradually. When the coarse aggregate particle size of the model is set as 5-40 mm, the capacity of damage resistance of concrete reaches the optimal. Therefore, it can be concluded that the minimum particle size will affect the dynamic damage performance of concrete. If the minimum particle size increases, the aggregate gradation quality in concrete will decrease, which will eventually lead to the decline in the internal strength of concrete and affect the damage resistance capacity of concrete.

4.4.2 The minimum particle size of coarse aggregate

This part will do the research on the influence of the maximum particle size of coarse aggregate on concrete damage. Under the condition of keeping the minimum particle size of coarse aggregate 5 mm unchanged, dynamic damage simulation was carried out on concrete specimen, and the maximum particle size distribution of coarse aggregate was in the range of 20-40 mm. As can be seen from Fig. 15, the damage value of concrete increases with the increase of ultrasonic stress amplitude. When the coarse aggregate size distributes in the range of 5-40 mm, the damage to concrete reaches the largest value. Meanwhile, concrete models with aggregate size of 5-20 mm have the strongest damage resistance ability. It shows that the maximum particle size of coarse aggregate will affect the dynamic damage behavior of concrete. With the maximum particle size of aggregate increasing gradually, the instability of concrete internal gradation increases which leads to the decline in the interior performance of concrete and anti-damage ability.

5. Conclusions

The dynamic damage process of concrete has been studied by the testing of ultrasonic concrete crushing and a three-dimensional random aggregate concrete model was adopted. The effects of different amplitudes of ultrasonic stress and the coarse aggregate particle size, as well as, coarse aggregate volume fraction were investigated. The conclusions are as follow:

• The ultrasonic dynamic loading is better than the static load. With the increase of amplitude of ultrasonic stress, the concrete interior stress increases and the damage process accumulates gradually. It is clear that the model size directly affects the peak stress of the concrete, and the larger the size, the lower the peak stress. At the same time, the peak stress of concrete with a volume fraction of 40% reached the maximum value, which prove an important size effect.
• In the concrete random aggregate model generated by APDL, concrete damage accumulates gradually over time. When the fraction of coarse aggregate reaches 40%, it has the best anti-damage ability and its internal stress performance becomes more stable.
• The experiment and simulation results showed that the maximum and minimum particle size of coarse aggregate affect the damage resistance of concrete. When the maximum particle size of coarse aggregate increases gradually, concrete is more vulnerable to damage.

Acknowledgments

The research described in this paper was financially supported by the National Natural Science Foundation of China (51705037).

References

Abdollahzadeh, G., Jahani, E. and Kashir, Z. (2016), "Predicting of compressive strength of recycled aggregate concrete by genetic programming", *Comput. Concrete*, **18**(2), 155-163. http://dx.doi.org/10.12989/cac.2016.18.2.155.

Abyaneh, S.D., Wong, H.S. and Buenfeld, N.R. (2013), "Modelling the diffusivity of mortar and concrete using a three-dimensional mesostructure with several aggregate shapes", *Comput. Mater. Sci.*, **78**, 63-73. https://doi.org/10.1016/j.commatsci.2013.05.024.

Al-Salloum, Y., Almusallam, T., Ibrahim, S.M., Abbas, H. and Alsayed, S. (2015), "Rate dependent behavior and modeling of concrete based on SHPB experiments", *Cement Concrete Compos.*, **55**, 34-44. https://doi.org/10.1016/j.cemconcomp.2014.07.011.

Alexandre, B.J. and Gomes, A. (2013), "Compressive behavior and failure modes of structural lightweight aggregate concrete - Characterization and strength prediction", *Mater. Des.*, **46**, 832-841. https://doi.org/10.1016/j.matdes.2012.11.004.

Anil, O., Durucan, C., Erdem, R.T. and Yorgancilar, M.A. (2016), "Experimental and numerical investigation of reinforced concrete beams with variable material properties under impact loading", *Constr. Build. Mater.*, **125**, 94-104. https://doi.org/10.1016/j.conbuildmat.2016.08.028.

Aoude, H., Dagenais, F.P., Burrell, R.P. and Saatcioglu, M. (2015), "Behavior of ultra-high performance fiber reinforced concrete columns under blast loading", *Int. J. Impact Eng.*, **80**, 185-202. https://doi.org/10.1016/j.ijimpeng.2015.02.006.

Asteris, P.G., Ashrafian, A. and Rezaie-Balf, M. (2019), "Prediction of the compressive strength of self-compacting concrete using surrogate models", *Comput. Concrete*, **24**(2), 137-150. https://doi.org/10.12989/cac.2019.24.2.137.

Bazant, Z.P. and Tabbara, M.R. (1990), "Random particle models for fracture of aggregate or fiber composites", *J. Eng. Mech.*, **116**(8), 1686-1705. https://doi.org/10.1061/(ASCE)0733-9399(1990)116:8(1686).

Cao, L., Liu, J.P. and Chen, Y.F. (2018), "Vibration performance of arch prestressed concrete truss girder under impulse excitation", *Eng. Struct.*, **165**, 386-395. https://doi.org/10.1016/j.engstruct.2018.03.050.

Chen, J.Q., Wang, H. and Li, L. (2017), "Virtual testing of asphalt mixture with two-dimensional and three-dimensional random aggregate structures", *Int. J. Pave. Eng.*, **9**(18), 824-836. https://doi.org/10.1080/10298436.2015.1066005.

Chen, J.Q., Wang, H., Dan, H.C. and Xie, Y.J. (2018), "Random modeling of three-dimensional heterogeneous microstructure of asphalt concrete for mechanical analysis", *J. Eng. Mech.*, **9**, 144. https://doi.org/10.1061/(ASCE)EM.1943-7889.0001505.

Du, X.L., Jin, L. and Ma, G.W. (2014), "Numerical simulation of dynamic tensile-failure of concrete at meso-scale", *Int. J. Impact Eng.*, **66**, 5-17. https://doi.org/10.1016/j.ijimpeng.2013.12.005.

Ganesan, N., Raj, J.B. and Shashikala, A.P. (2013), "Flexural fatigue behavior of self compacting rubberized concrete", *Constr. Build. Mater.*, **44**, 7-14. https://doi.org/10.1016/j.conbuildmat.2013.02.077.

Gholipour, G., Zhang, C.W. and Mousavi, A.A. (2019), "Loading rate effects on the responses of simply supported RC beams subjected to the combination of impact and blast loads", *Eng. Struct.*, **201**, 109837. https://doi.org/10.1016/j.engstruct.2019.109837.

Gultop, T., Yilmaz, M.C. and Alyavuz, B. (2015), "An analytical investigation of rigid plastic beams under impact loading", *J. Facul. Eng. Arch. Gazi Univ.*, **1**(30), 87-94.

Heravi, A.A., Curosu, I. and Mechtcherine, V. (2020), "A gravity-driven split Hopkinson tension bar for investigating quasi-ductile and strain-hardening cement-based composites under tensile impact loading", *Cement Concrete Compos.*, **105**, UNSP 103430. https://doi.org/10.1016/j.cemconcomp.2019.103430

Huang, Y.J., Yang, Z.J., Ren, W.Y., Liu, G.H. and Zhang, C.Z. (2015), "3D meso-scale fracture modelling and validation of concrete based on in-situ X-ray computed tomography images using damage plasticity model", *Int. J. Solid. Struct.*, **67-68**, 340-352. https://doi.org/10.1016/j.ijsolstr.2015.05.002.

Jin, R.Y. and Chen, Q. (2019), "Overview of concrete recycling legislation and practice in the United States", *J. Constr. Eng. Manage.*, **4**, 145. https://doi.org/10.1061/(ASCE)CO.1943-7862.0001630.

Kalinowska, W.K., Pawluczuk, E. and Boltryk, M. (2020), "Waste-free technology for recycling concrete rubble", *Constr. Build. Mater.*, **234**, UNSP 117407. https://doi.org/10.1016/j.conbuildmat.2019.117407.

Kaliyavaradhan, S.K. and Ling, T.C. (2017), "Potential of CO2 sequestration through construction and demolition (C&D) waste –An overview", *J. CO_2 Utiliz.*, **20**, 234-242. https://doi.org/10.1016/j.jcou.2017.05.014.

Kim, J.R., Kwak, H.G. and Kim, B.S. (2019), "Finite element analyses and design of post-tensioned anchorage zone in ultra-high-performance concrete beams", *Adv. Struct. Eng.*, **22**(2), 323-336. https://doi.org/10.1177/1369433218787727.

Kim, K., Bolander, J.E. and Lim, Y.M. (2013), "Failure simulation of RC structures under highly dynamic conditions using random lattice models", *Comput. Struct.*, **125**, 127-136. https://doi.org/10.1016/j.compstruc.2013.04.007.

Kwak, H.G. and Gang, H.G. (2015), "An improved criterion to minimize FE mesh-dependency in concrete structures under high strain rate conditions", *Int. J. Impact Eng.*, **86**, 84-95. https://doi.org/10.1016/j.ijimpeng.2015.07.008.

Li, Y., Algassem, O. and Aoude, H. (2018), "Response of high-strength reinforced concrete beams under shock-tube induced blast loading", *Constr. Build. Mater.*, **189**, 420-437. https://doi.org/10.1016/j.conbuildmat.2018.09.005.

Liang, S.X., Chen, J.S., Li, J., Lin, S.P., Chi, S.W., Hillman, M., Roth, M. and Heard, W. (2017), "Numerical investigation of statistical variation of concrete damage properties between scales", *Int. J. Fract.*, **208**(1-2), 97-113. https://doi.org/10.1007/s10704-017-0217-z.

Liu, H.F. and Ning, J.G. (2009), "Mechanical behavior of reinforced concrete subjected to impact loading", *Mech. Mater.*, **41**(12), 1298-1308. https://doi.org/10.1016/j.mechmat.2009.05.008.

Liu, H.F., Fu, J. and Ning, J.G. (2016), "Experimental study on the dynamic mechanical properties of reinforced concrete under shock loading", *Acta Mechanica Solida Sinica*, **29**(1), 253-261. https://doi.org/10.1016/S0894-9166(16)60004-6.

Liu, H.K., Ren, X.D., Liang, S.X. and Li, J. (2019), "Physical mechanism of concrete damage under compression", *Mater. (Basel, Switzerland)*, **12**(20), 3295. https://doi.org/10.3390/ma12203295.

Lotfi, S., Eggimann, M., Wagner, E., Mroz, R. and Deja, J. (2015), "Performance of recycled aggregate concrete based on a new concrete recycling technology", *Constr. Build. Mater.*, **95**, 243-256. https://doi.org/10.1016/j.conbuildmat.2015.07.021.

Matzenmiller, A., Lubliner, J. and Taylor, R.L. (1995), "A constitutive model for anisotropic damage in fiber-composites", *Mech. Mater.*, **20**(2), 125-152. https://doi.org/10.1016/0167-6636(94)00053-0.

Nakahata, K., Kawamura, G., Yano, T. and Hirose, S. (2015), "Three-dimensional numerical modeling of ultrasonic wave propagation in concrete and its experimental validation", *Constr. Build. Mater.*, **78**, 217-223. https://doi.org/10.1016/j.conbuildmat.2014.12.049.

Nam, J.W., Choi, H.J., Kim, J.H.J., Kim, I.S., Yi, N.H. and Kim, H.J. (2009), "Blast analysis of concrete arch structures for FRP retrofitting design", *Comput. Concrete*, **6**(4), 305-318. https://doi.org/10.1016/j.conbuildmat.2014.12.049.

Saleem, M. and Nasir, M. (2016), "Bond evaluation of steel bolts for concrete subjected to impact loading", *Mater. Struct.*, **49**(9), 3635-3646. https://doi.org/10.1617/s11527-015-0745-9.

Salesa, A., Perez, B.J.A., Esteban, L.M., Vicente, V.R. and Orna, C.M. (2017), "Physico-mechanical properties of multi-recycled self-compacting concrete prepared with precast concrete rejects", *Constr. Build. Mater.*, **153**, 364-373. https://doi.org/10.1016/j.conbuildmat.2017.07.087.

Skarzynski, L., Nitka, M. and Tejchman, J. (2015), "Modelling of concrete fracture at aggregate level using FEM and DEM based on X-ray mu CT images of internal structure", *Eng. Fract. Mech.*, **147**, 13-35. https://doi.org/10.1016/j.engfracmech.2015.08.010.

Smith, J., Cusatis, G., Pelessone, D., Landis, E., O'Daniel, J. and Baylot, J. (2014), "Discrete modeling of ultra-high-performance concrete with application to projectile penetration", *Int. J. Impact Eng.*, **65**, 13-32. https://doi.org/10.1016/j.ijimpeng.2013.10.008.

Tahmouresi, B., Koushkbaghi, M., Monazami, M., Abbasi, M.T. and Nemati, P. (2019), "Experimental and statistical analysis of hybrid-fiber-reinforced recycled aggregate concrete", *Comput Concrete*, **24**(3), 193-206. https://doi.org/10.12989/cac.2019.24.3.193.

Tehrani, F.F., Absi, J., Allou, F. and Petit, C. (2013), "Investigation into the impact of the use of 2D/3D digital models on the numerical calculation of the bituminous composites' complex modulus", *Comput. Mater. Sci.*, **79**, 377-389. https://doi.org/10.1016/j.commatsci.2013.05.054.

Wang, X.F., Yang, Z.J. and Jivkov, A.P. (2015), "Monte Carlo simulations of mesoscale fracture of concrete with random aggregates and pores: a size effect study", *Constr. Build. Mater.*, **80**, 262-272. https://doi.org/10.1016/j.conbuildmat.2015.02.002.

Wang, X.F., Yang, Z.J. and Yates, J.R. (2015), "Jivkov, AP. Zhang, C. Monte Carlo simulations of mesoscale fracture modelling of concrete with random aggregates and pores", *Constr. Build. Mater.*, **75**, 35-45. https://doi.org/10.1016/j.conbuildmat.2014.09.069.

Wittmann, F.H. and Roelfstra, P.E. (1988), "Drying of concrete: An application of the 3L approach", *Nucl. Eng. Des.*, **105**, 185-198. https://doi.org/10.1016/0029-5493(88)90339-1.

Wu, J., Ning, J.G. and Ma, T.B. (2017), "The dynamic response and failure behavior of concrete subjected to new spiral projectile impacts", *Eng. Fail. Anal.*, **79**, 547-564. https://doi.org/10.1016/j.engfailanal.2017.05.037.

Xiang, Y., Fang, Z. and Fang, Y.W. (2017), "Single and multiple impact behavior of CFRP cables under pretension", *Constr. Build. Mater.*, **140**, 521-533. https://doi.org/10.1016/j.conbuildmat.2017.02.112.

Yu, R., Spiesz, P. and Brouwers, H.J.H. (2014), "Static properties and impact resistance of a green Ultra-High Performance Hybrid Fibre Reinforced Concrete (UHPHFRC): Experiments and modeling", *Constr. Build. Mater.*, **68**, 158-171. https://doi.org/10.1016/j.conbuildmat.2014.06.033.

Zhang, J., Li, J. and Woody, J. (2016), "3D elastoplastic damage model for concrete based on novel decomposition of stress". *Int. J. Solid. Struct.*, **94-95**, 125-137. https://doi.org/10.1016/j.ijsolstr.2016.04.038.

Zhang, Z.H., Cao, F., Yang, J.Y. and He, Z.G. (2018), "Experiment on natural frequency change of reinforced concrete members under low cycle loading", *Shock Vib.*, **2018**, 6504519. https://doi.org/10.1155/2018/6504519.

Zhou, W., Tang, L.W., Liu, X.H., Ma, G. and Chen, M.X. (2016), "Mesoscopic simulation of the dynamic tensile behaviour of concrete based on a rate-dependent cohesive model". *Int. J. Impact Eng.*, **95**, 165-175. https://doi.org/10.1016/j.ijimpeng.2016.05.003.

CC